Materials Characterization 171 (2021) 110778

Contents lists available at ScienceDirect

Materials Characterization

journal homepage: www.elsevier.com/locate/matchar

Elemental redistribution and precipitation reactions of 9Cr1.5Mo1CoB (FB2) steel during tempering

Yongqiang Zhang, Jianfeng Gu *, Lizhan Han *

Institute of Materials Modification and Modelling, Shanghai Jiao Tong University, Shanghai 200240, China

ARTICLE INFO

Keywords:
Tempering
Elemental redistribution
Precipitation reactions

ABSTRACT

The effect of tempering temperature on the precipitation reactions and elemental redistribution in 9Cr1.5Mo1CoB(FB2) steel has been studied using scanning electron microscope(SEM), transmission electron microscope(TEM), secondary ion mass spectrometry(Tof-SIMS) and atom probe technique (APT). The results show that water-cooling from normalization at 1100 °C produced lathy martensite. During tempering at 500 °C, only C and B atoms were segregated, and formed needle-like $Fe_3(C, B)$; After tempering at 600 °C, the segregation of Cr, Mo and Mn showed noticeable difference, forming Cr + Mn + Mo + C + B and Mo + Cr + C + B clusters. Consequently, $(Cr,Mo)_2(C,B)$, Cr-rich $M_7(C,B)_3$ and Cr-rich $M_{23}(C,B)_6$ were observed in sample tempered at 600 °C. And both $(Cr,Mo)_2(C,B)$ and $M_7(C,B)_3$ particles were entirely replaced by Cr-rich $M_{23}(C,B)_6$ by enhancing the tempering temperature to 700 °C. Therefore, the evolution of carbides in FB2 steel during tempering at 500 °C–700 °C can be summarised as follows: $Fe_3(C,B) \rightarrow (Cr,Mo)_2(C,B)$ + Cr-rich $M_7(C,B)_3 \rightarrow$ Cr-rich $M_{23}(C,B)_6$. Besides, the Mo element in (V,Nb,Mo)(N,C) particles was gradually replaced by V and Nb with the increase of temperature from 600 °C to 700 °C. While Si and Co were rejected to the interfaces of carbides/matrix during tempering, forming a flux of Si and Co. Then, this flux may suppress carbides coarsening by retarding the diffusion of Cr, Mo and Mn from the matrix into carbides.

1. Introduction

9Cr1Mo martensitic heat resistant steels are widely used as thick-section components in the ultra-supercritical electric generator(USC) power plant due to its excellent creep strength and high-temperature oxidation resistance [1]. Normally, the heat treatment process for these components consists of normalizing and tempering. During tempering, the redistribution of elements, the precipitation reactions and the evolution of substructures eventually determine the mechanical properties [1,2]. Thus, by understanding these aspects at the microstructural level, alloy tailoring can be achieved, whereby improved mechanical properties allow for greater flexibility in designing structural components.

As widely reported, the precipitation of carbides in 9Cr1Mo steels during tempering is closely related to the chemical composition of steels and the heat treatment process [2]. K. Kaneko [3] suggests that only Fe_3C or M_3C forms at 300–500 °C, while some studies [4,5] show that M_2C and M_7C_3 were observed in 9-12Cr steel after tempered at 300 °C. By enhancing the tempering temperature to 600 °C–780 °C, these carbides involve in different sequences of $M_3C \rightarrow M_2C \rightarrow M_7C_3 + M_6C \rightarrow M_{23}C_6$ [5], $M_3C \rightarrow M_2C \rightarrow M_7C_3 + M_{23}C_6 \rightarrow M_{23}C_6 + M_6C$ [6] or $M_3C \rightarrow M_2C \rightarrow M_{23}C_6 + M_6C$ [7]. These disagreements of carbides evolution may be closely related to tempering process and material compositions, because the formation of carbides depends on its thermal stability and the redistribution behavior of elements such as Cr, Mo and Mn during tempering.

For B containing steels, J. Takahashi [8] suggested experimentally the segregation of C and B to the interfaces of martensitic lath and prior-austenite grain boundaries(PAGBs) during quenching by atomic probe technique(APT). And then, these B atoms diffuse from the PAGBs to the matrix during tempering [9]. Meanwhile, it is reported that B atoms can also enter the carbides during tempering, forming M_2B [10]. For non-carbide forming elements such as Si and Co, many studies have been indicated that both elements can influence the morphology and distribution of precipitates during tempering [11–14]. It is a well-established fact that Si plays a retarding effect on the epsilon to cementite carbide transition in tempered martensitic steels by forming as a growth barrier to inhibit the cementite precipitation [11]. Dong [12] and Delagnes [13]

* Corresponding author.
E-mail addresses: gujf@sjtu.edu.cn (J. Gu), victory_han@sjtu.edu.cn (L. Han).

https://doi.org/10.1016/j.matchar.2020.110778
Received 17 July 2020; Received in revised form 4 November 2020; Accepted 21 November 2020
Available online 25 November 2020

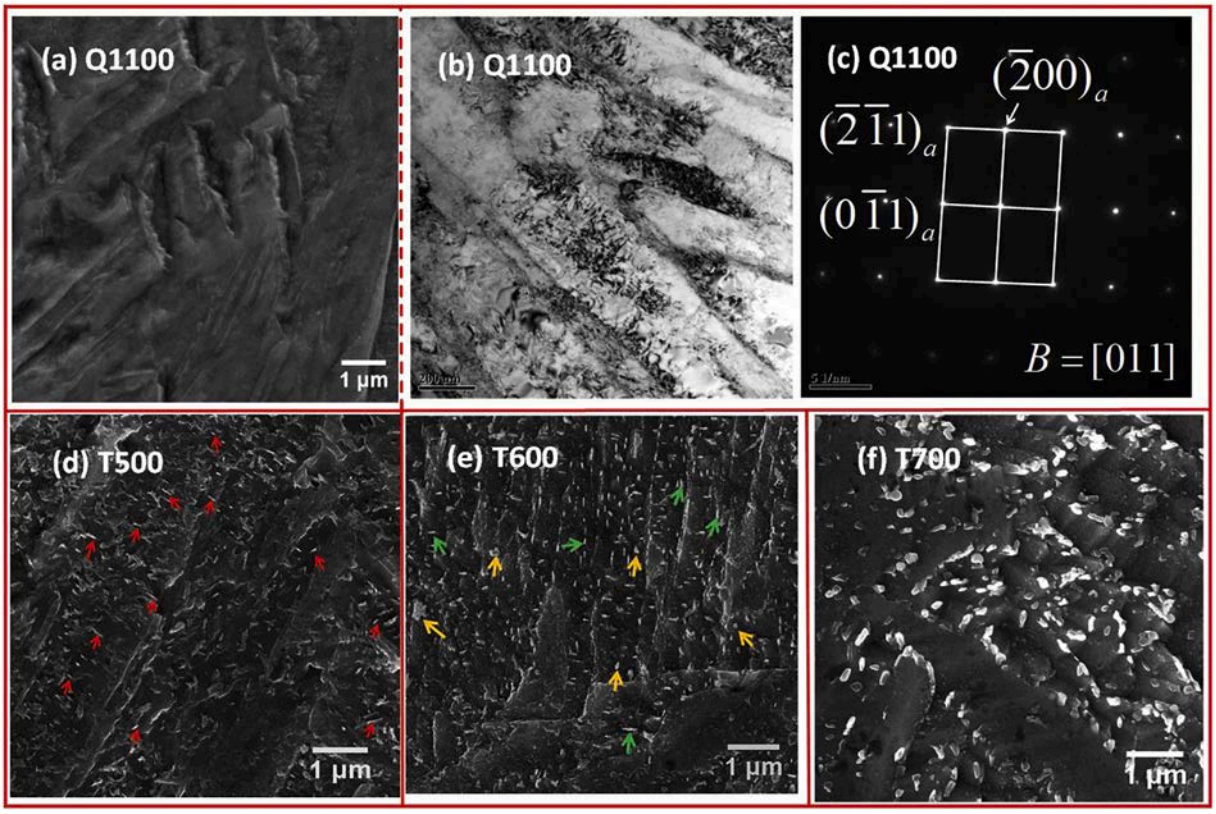

Fig. 1. (a-c) SEM, TEM micrographs and selected area electron diffraction (SAED) pattern of Q1100 sample, respectively, (d-f) SEM micrographs of T500, T600 and T700 samples.

proposed that Si also affects the formation of MX, M_7C_3 and $M_{23}C_6$. It has long been known that Co addition increases the resistance to tempering softening in steels by slowing particle coarsening [14,15]. In addition, carbide-forming elements (Mo, Nb, V) influencing the precipitation kinetics were added to 9Cr steels, resulting in a significant effect on the secondary hardening peak [16]. These above results indicate that the precipitation and elemental redistribution is inseparable during tempering.

However, a systematic study of carbide precipitation, elemental redistribution, and the elements partitioning at carbides/martensite interfaces during tempering at different temperatures of 9Cr1.5Mo1CoB steel has not been done in details. In this study, the elemental redistribution and precipitation reactions of 9Cr steel were studied using SEM, TEM, Tof-SIMS and APT. The purpose of this study is to clarify the effect of tempering temperature on elemental redistribution and the precipitation reactions. The research may contribute to a greater understanding of the microstructure evolution during tempering.

2. Material and experimental procedure

The chemical composition of FB2 steel is Fe0.14C 9.06Cr1.15Co1.51Mo0.42Mn0.21V0.053Nb0.06Si0.17Ni0.008 B0.06 N (wt%). The as-received FB2 steel forged pieces in the tempered state were cut into cubes (100 × 100 × 15 mm) by wire electric spark cutting machine. All these cubes were homogenized at 1100 °C for 10 h and then by water cooling to room temperature(named Q1100). Subsequently, tempering treatments at 500 °C, 600 °C and 700 °C for 2 h were carried out and cooled in water to room temperature(named T500, T600 and T700, respectively).

The specimens for SEM observation were metallographically

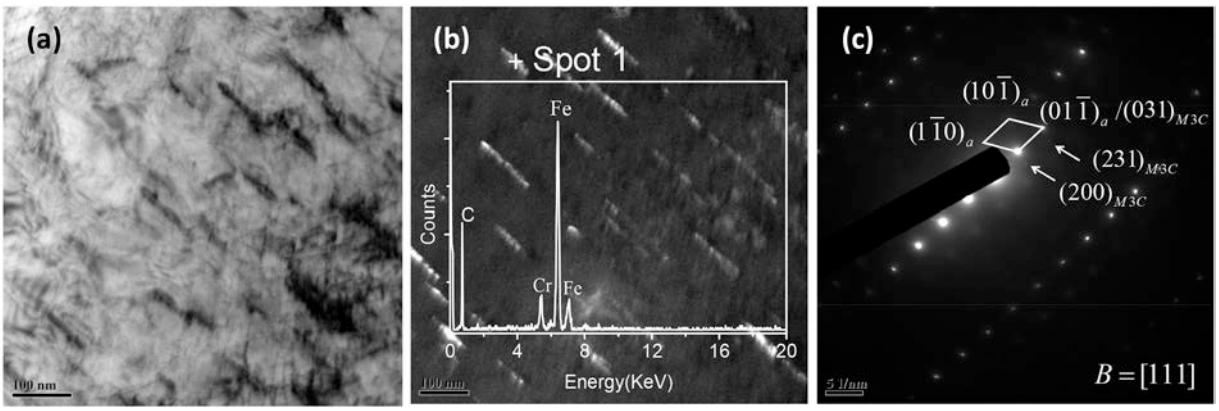

Fig. 2. M_3C carbide in T500 sample: (a) bright-field(BF) image, (b) dark-field(DF) image and Energy spectrum(EDS), (c) SAED pattern.

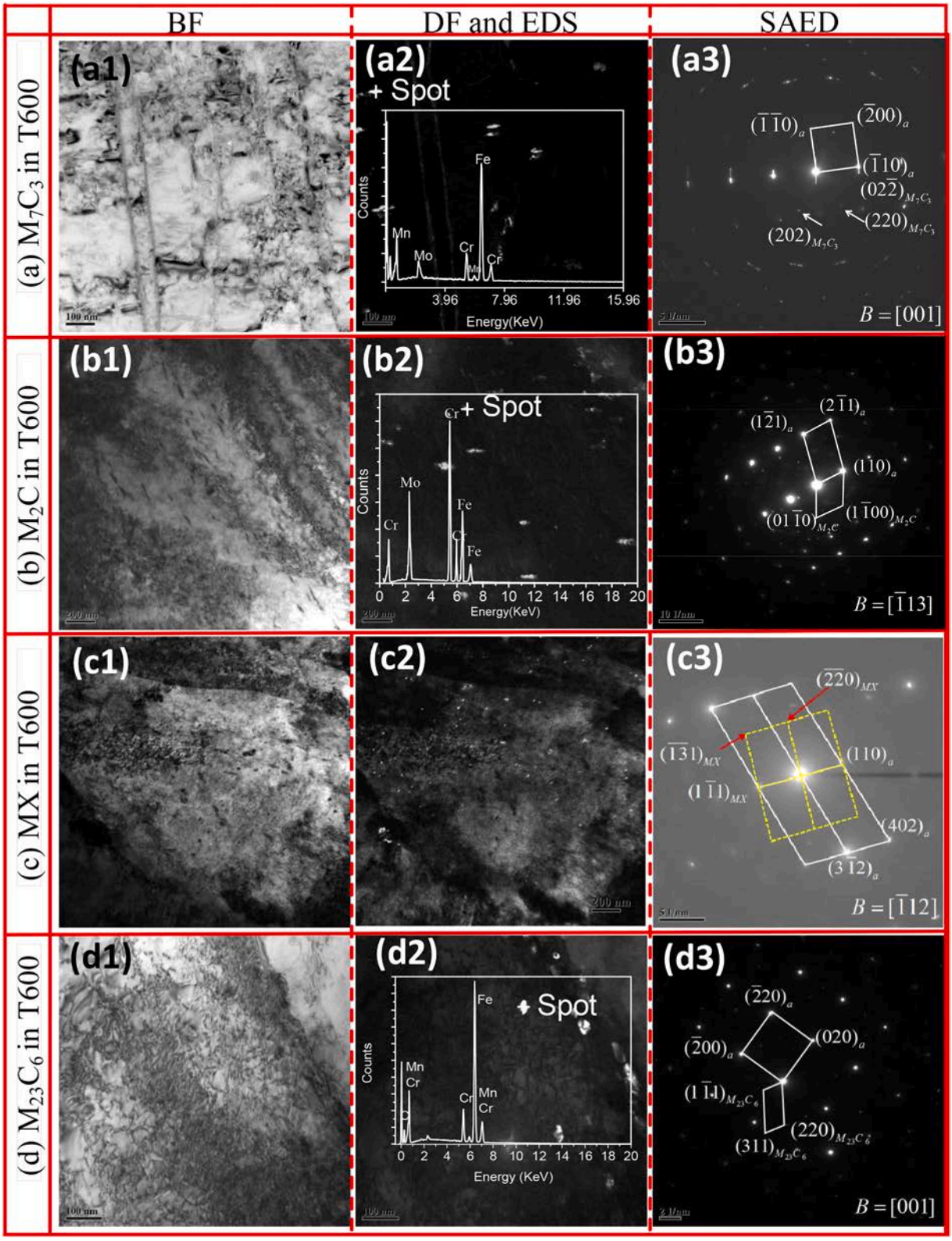

Fig. 3. BF image, DF image, SAED pattern and EDS of precipitates in FB2 steel in T600 condition: (a) M_7C_3, (b) M_2C, (c) MX and (d) $M_{23}C_6$.

prepared and then etched in the solution of 5 g $FeCl_3$, 19 ml hydrochloric acid, and 100 ml deionized water for 5 s. The TEM foils were prepared using the double jet electro-polishing method with a 7% solution of perchloric acid in ethyl alcohol and a voltage of 35 V at the temperature of −25 °C. Subsequently, TEM observations were performed on a JEM-2100F instrument at an operating voltage of 200 kV.

The tempered samples were further detected for elements distribution using atom probe technique(APT) and secondary ion mass spectrometry(Tof-SIMS). For APT observation, specimens were electro-polished with the standard double-layer and micro-polishing methods [17]. Subsequently, the APT analysis was performed using the LEAP 3000X HR instrument operated with a specimen temperature of 60 K, a

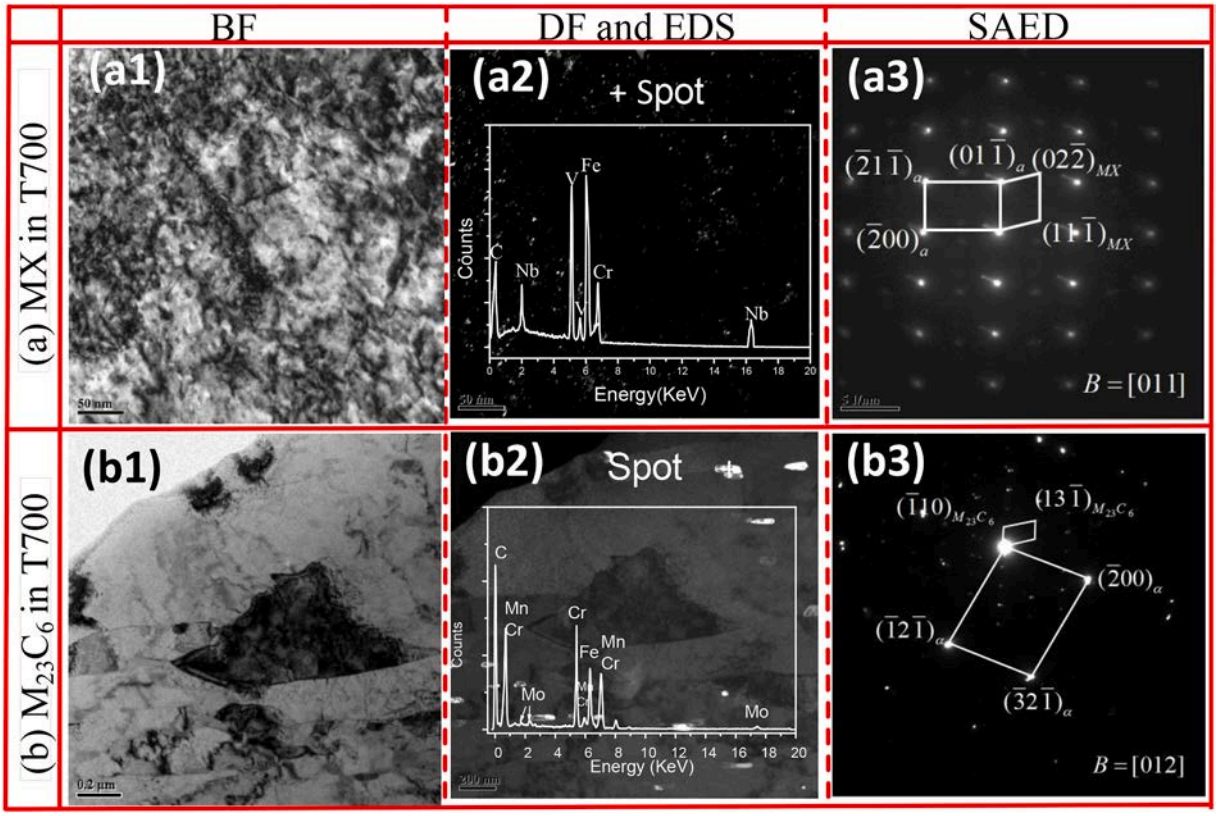

Fig. 4. Bright-field image(BF), dark-field image(DF), selective electron diffraction(SAED) and Energy spectrum(EDS) of precipitates in FB2 steel in T700 condition. (a1-a3) MX particles, (b1-b3) $M_{23}C_6$ particles.

pulse repetition rate of 200 kHz, and a pulse fraction of 20% [17]. The obtained data were reconstructed using the IVAS 3.6.2 software to analyze the distribution of elements. The SIMS experiment by using ToF SIMS 5–100 was conducted to detect the elemental distribution.

3. Experimental results

3.1. SEM and TEM micrographs

Fig. 1 shows the SEM and TEM observations of Q1100, T500, T600 and T700 samples. As can be seen from Fig. 1a-c, no precipitates were observed in the Q1100 sample, which indicates that the water-cooling can inhibit the self-tempering of FB2 steel. After tempering at 500 °C, the spin-like precipitates were observed in the T500 condition(Fig. 1d). While two types of particles(rod-like and spheroidal carbides indicated by green and yellow arrows, respectively) were observed in the T600 condition, as shown in Fig. 1e. With increasing tempering temperature to 700 °C, the matrix was decorated with large spherical precipitates along the martensite lath interfaces (Fig. 1f).

3.2. TEM observation of precipitates in T500-T700 samples

Fig. 2 shows the TEM micrographs of sample tempered at 500 °C. The spin-like precipitates observed within martensite lath in T500 condition were identified as Fe-rich M_3C with the lattice constant (a = 5.091 nm, b = 6.743 nm, c = 4.526 nm) based on the SAED pattern and the EDS spectrum [18].

In the case of T600, four types of precipitates with different morphologies (rod-like, shuttle-like, fine globular and large globular particles) were identified based on the TEM observations, as shown in Fig. 3a-d. The rod-like particles with similar morphology as M_3C in T500 condition were observed within laths (Fig. 3a). The BF image, DF image, SAED pattern, and EDS analysis indicate that these particles are Cr-rich M_7C_3 with an orthorhombic system(a = 0.701 nm, b = 1.215 nm, c = 0.4532 nm) [19]. The shuttle-shape particles with an average size of 50 nm are considered to be M_2C with a hexagonal structure, and the lattice parameters estimated corresponding to the SAED in Fig. 3b2 to be a = 0.4805 nm and c = 0.4476 nm respectively [20]. Further, EDS analysis shows signals characteristic of Mo and Cr, which indicates the shuttle-like particles were $(Cr, Mo)_2C$.

Another type of fine spherical carbides with an average size of 22 nm distributed within martensitic lath, as shown in Fig. 3c1-3c3. And SAED pattern and DF image indicate that these fine particles are MX carbides with a face-centered cubic structure(a = 1.065 nm). While according to SAED and EDS analysis, the large spherical particles have a face-centered cubic structure (a = 1.065 nm) and contain Cr, Mo, Fe, and Mn, as shown in Fig. 3d1-3d3. Therefore, it can be determined from these results that the these large particles were Cr-rich $M_{23}C_6$ [16,21].

In the T700 condition, large and fine particles were observed, as shown in Fig. 4. Fig. 4a gives the BF and DF micrographs showing the distribution of fine particles in the matrix. These fine particles were determined by EDX and SAED analysis as V-rich MX with a face-centered cubic structure(a = 0.4139 nm) [17]. And the large particles have a face-centered cubic structure(a = 1.068 nm), which is considered as Cr-rich $M_{23}C_6$ carbides [20], as shown in Fig. 4b.

3.3. Elemental redistribution in FB2 steel during tempering

3.3.1. Elemental distribution of T500

Fig. 5a-e shows the isoconcentration surface(ICS) of 1.8 at.% C, 0.6 at.% B atoms and the atomic distribution of Cr, Mo and Mn in the T500 condition. It can be seen that the C-clusters randomly dispersed throughout the matrix(Fig. 5e), which has been attributed to C atoms segregation to dislocations, martensite lath boundaries, or original austenite boundaries to form the Cottrell atmospheres or carbides [21]. While no partitioning of Cr, Mn, Co and Mo into the C-enriched regions

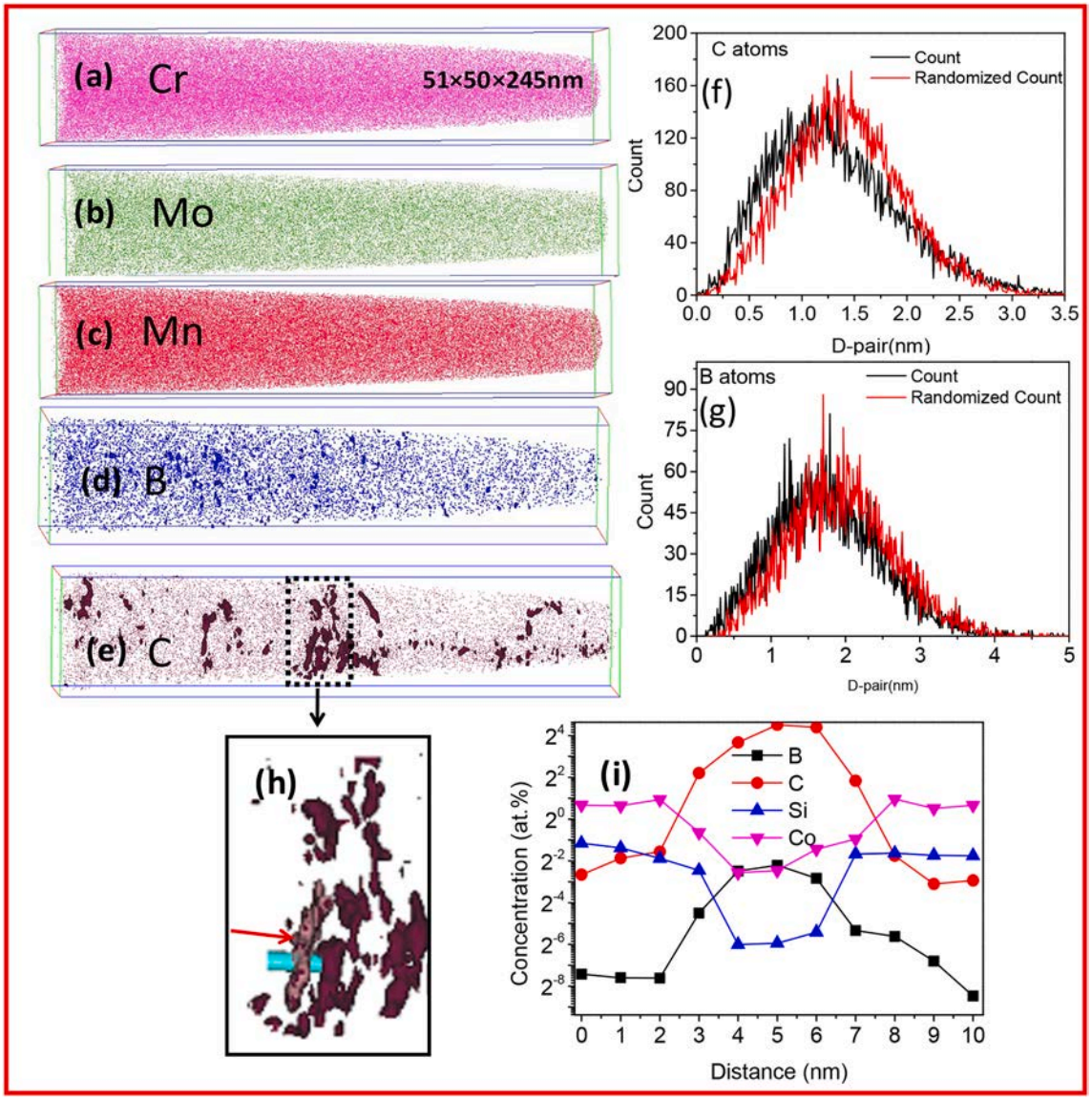

Fig. 5. APT analysis of T500 sample: (a-c) atom maps showing the alloy atoms distribution of Cr, Mn and Mo, (d-e) the isoconcentration surface (ICS) of 0.6 at.% B and 1.8 at.% C, (f-g) the nearest-neighbor distribution(NND) curves of C and B, (h) the enlarged volume in Fig. 5e and an intercepted cylinder, (i) the variation of element concentrations along the axis of the cylinder in Fig. 5h.

(Fig. 5a-c). Fig. 5f-g further shows the nearest-neighbor distribution (NND) curves of C and B. Clearly, experimental results are not identical with that of theoretical distribution for C and B. These results strongly suggest that the segregation of C and B can occur during tempering at 500 °C, while Cr, Mo and Mn are uniformly distributed in the matrix.

In addition, it can be seen from the ICS of B and C that both elements have identical distribution(Fig. 5d-e). Takahashi [8] holds that B atoms only segregate at the original austenite boundary during quenching by non-equilibrium grain-boundary segregation. Then, the B atoms will diffuse into the matrix again during tempering [9]. In this experiment, although we cannot determine the distribution of B atoms after quenching, there is no doubt that both B and C occupy the same spatial position in the detected volume. To further explore the distribution of elements in detail, a cylinder with a diameter of Ø3nm × 10 nm was cut from the reconstructed ICS of C atoms (Fig. 5e-h). And its elemental concentration variation along the arrow direction is shown in Fig. 5i. The results from Fig. 5i indicate that the highest segregation concentration of C and B are 22.3 at.% and 0.21 at.%. In contrast, the mean atomic concentration of B and C in the matrix is 31.3 ppm and 0.0736 at.%, respectively. Besides, Si and Co elements are depleted in the carbon-rich region. And the maximum enrichment concentration of Si and Co at the carbon-rich region/matrix interface is 0.38 at.% and 1.92 at.%, respectively, higher than the average concentration of Si and Co in the matrix.

3.3.2. *Elemental distribution of T600*

Fig. 6 shows the NND curves and atoms distribution of Cr, Mn, Mo, C and B in the T600 condition. From the NND curves (Fig. 6a), it is observed that the misalignment of experimental statistics results and theoretical distribution for Cr, Mn, and Mo, which indicate that these elements are not uniformly distributed in the matrix. From Fig. 6b-d, the co-segregation of Cr, Mn, and Mo was observed, while Mo is not entirely distributed in this way. Except for the co-segregation of Cr + Mn + Mo + C(indicated by the green arrow in Fig. 6b-e), part of Mo atoms appeared in the Mn and Cr-deficient region, forming the Mo + C + B clusters (indicated by the black arrow in Fig. 6d-e).

In order to further study the chemical composition in these two clusters mentioned above, the ICS of 1.8 at.% C atoms were reconstructed, as shown in Fig. 7a-c. And then, two representative cylinders (named Cy1 and Cy2) were extracted from the ICS, which are

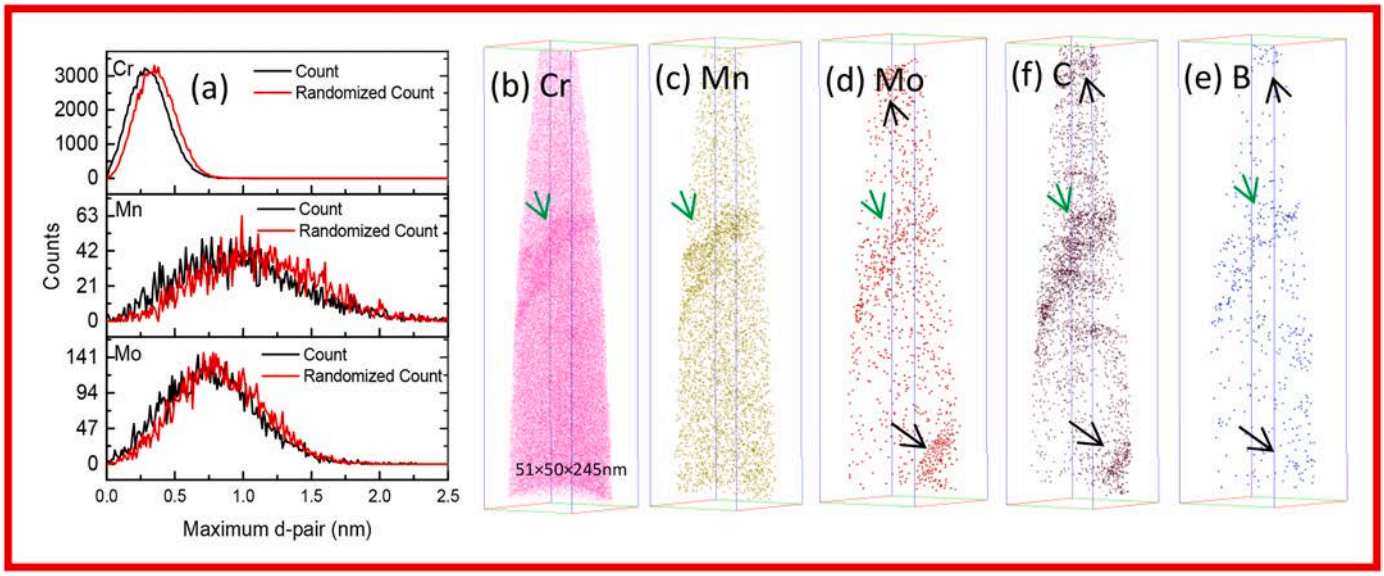

Fig. 6. (a) NND curves of Cr, Mn and Mo elements, (b-e) Atom maps showing atoms distribution of Cr, Mn, Mo, C and B in FB2 steel after tempered at 600 °C.

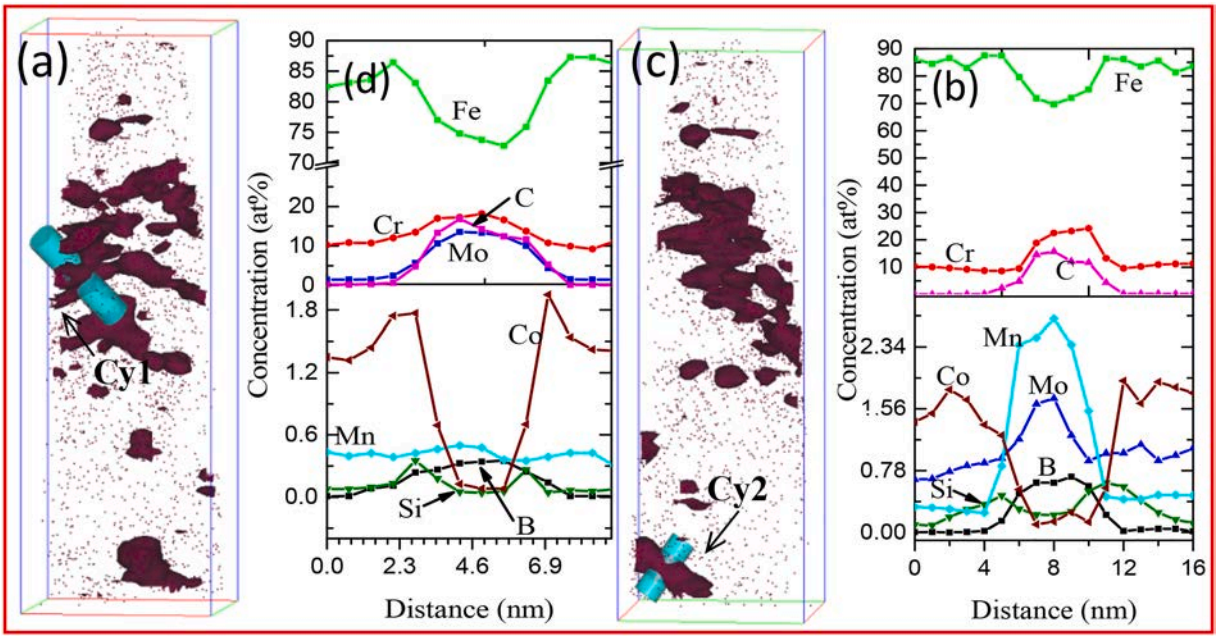

Fig. 7. (a, c) The reconstructed ICS of 1.8 at.%C and the intercepted cylinders(Cy1 and Cy2), (b, d) the elemental distribution along the axis of Cy1 and Cy2, respectively.

corresponding to the clusters of Cr + Mn + Mo + C + B and Mo + C + B, respectively. Fig. 7b and Fig. 7d show the elemental concentration variation of Cy1 and Cy2 along the axial direction, respectively. It was observed from Fig. 7b that the maximum atomic concentrations in Cy1 is 24.17Cr2.61Mn1.63Mo12.58C0.26B(at.%), indicating that the co-segregation of Cr, Mn and Mo. Besides, the depletion and the enrichment of Co and Si elements are observed inside and around the C clusters, respectively. According to the elemental concentration of Cy2 (Fig. 7d), the maximum atomic concentration is 17.45Cr0.47Mn11.46Mo14.22C0.61B(at.%), while the atomic concentration of Co and Si at C cluster/matrix interface is 1.94 at.%, 0.34 at.%, respectively.

Fig. 8a shows the reconstructed 1.2 at.% ICS of V in the T600 condition. V clusters were dispersed in the matrix, indicating that V segregation occurs after tempering at 600 °C. NND curve of V in Fig. 8b further prove that V elements are not evenly distributed in the matrix. In order to further investigate the chemical composition in V clusters, a cylinder(Ø3nm × 10 nm) was intercepted from the ICS of V, as shown in Fig. 8a. And the variation of elements concentration along the direction indicated by the arrow, as shown in Fig. 8c. The concentration profile (Fig. 8c) illustrates that the Nb, Mo, N, and C are rich in the V-cluster. And the maximum atomic concentration of V-cluster can be expressed as 31.67V4.72Nb14.42Mo36.56N13.45C(at.%), which further indicates that very fine MX precipitates observed in the above TEM analysis (Fig. 3c) are rich in these elements.

3.3.3. *Elemental distribution of T700*

Fig. 9a and Fig. 9b-f show SEM images including maps scanning of T700. It can be seen from Fig. 9a that most precipitates located at the martensitic lath interfaces, while a small number of spherical

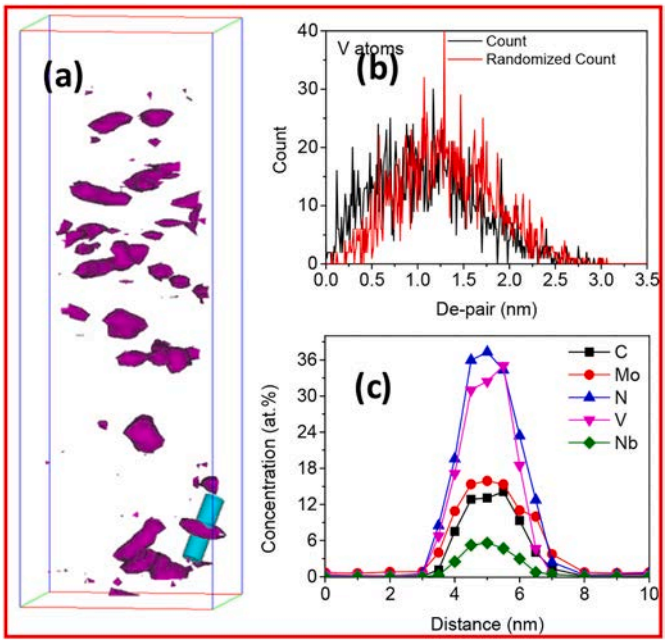

Fig. 8. (a) The reconstructed ICS of V element, (b) NND curves of V, (c) The variation of element concentrations along the axis of the cylinder in Fig. 8a.

precipitates distributed within the lath. According to the elemental distribution in Fig. 9b-f, it can be determined that some MX particles rich in Nb, V, Mo and C(circled in Fig. 9b-f), and $M_{23}C_6$ contains a large amount of Cr, Mo and C.

Fig. 10 shows the concentration profile of T700. From Fig. 10a-c, it is clear that clusters of V + Nb + Mo with an average size of 5–10 nm dispersed in the matrix. To quantitatively analyze the composition of this clusters, the ICS of the 1.2 at.% V is reconstructed. And then, a cylinder(Ø3nm × 10 nm) is extracted from the ICS, as shown in Fig. 10d. Fig. 10e shows the variation of elements concentration along the direction indicated by the arrow. The concentration of V clusters is mainly enriched in Mo, Nb and C, and the maximum chemical components are 37.48 V4.76Nb6.38Mo 35.58 N13.85C(at.%). Since the atomic ratio of V + Nb + Mo and C + N is close to 1:1, it can further be determined that these clusters are MX precipitates, which agrees well with the result of TEM (Fig. 4a).

To study the distribution of B atoms in T700, the SIMS was applied. The result in Fig. 11 show that B and Cr are enriched in spherical carbides. From TEM results (Fig. 4), only MX and $M_{23}C_6$ carbides were observed in the T700 condition. And these large spherical particles are thought to be Cr-rich $M_{23}C_6$ carbides. Thus, it can be concluded that B atoms are enriched in $M_{23}C_6$ carbides, forming Cr-rich $M_{23}(C, B)_6$.

4. Discussion

4.1. Precipitation sequence during tempering

The results of the above investigation show that the precipitation and the elemental redistribution behavior largely depend on the tempering temperature. The microstructure of the water-quenched sample is lathy martensite. After tempered at 500 °C, only M_3C particles were found. While M_2C, M_7C_3, $M_{23}C_6$ and MX formed above 600 °C, and both M_2C and M_7C_3 were replaced by $M_{23}C_6$ and MX with the increase of temperature to 700 °C.

No precipitates were found in the Q1100 sample, indicating that water-cooling is totally suppressed the formation of carbides. After tempered at 500 °C, a large number of needle-like M_3C type particles were found within martensitic lath. And the results of EDS(Fig. 2b) and APT(Fig. 5i) further show that these particles are rich in Fe, C and B. X-

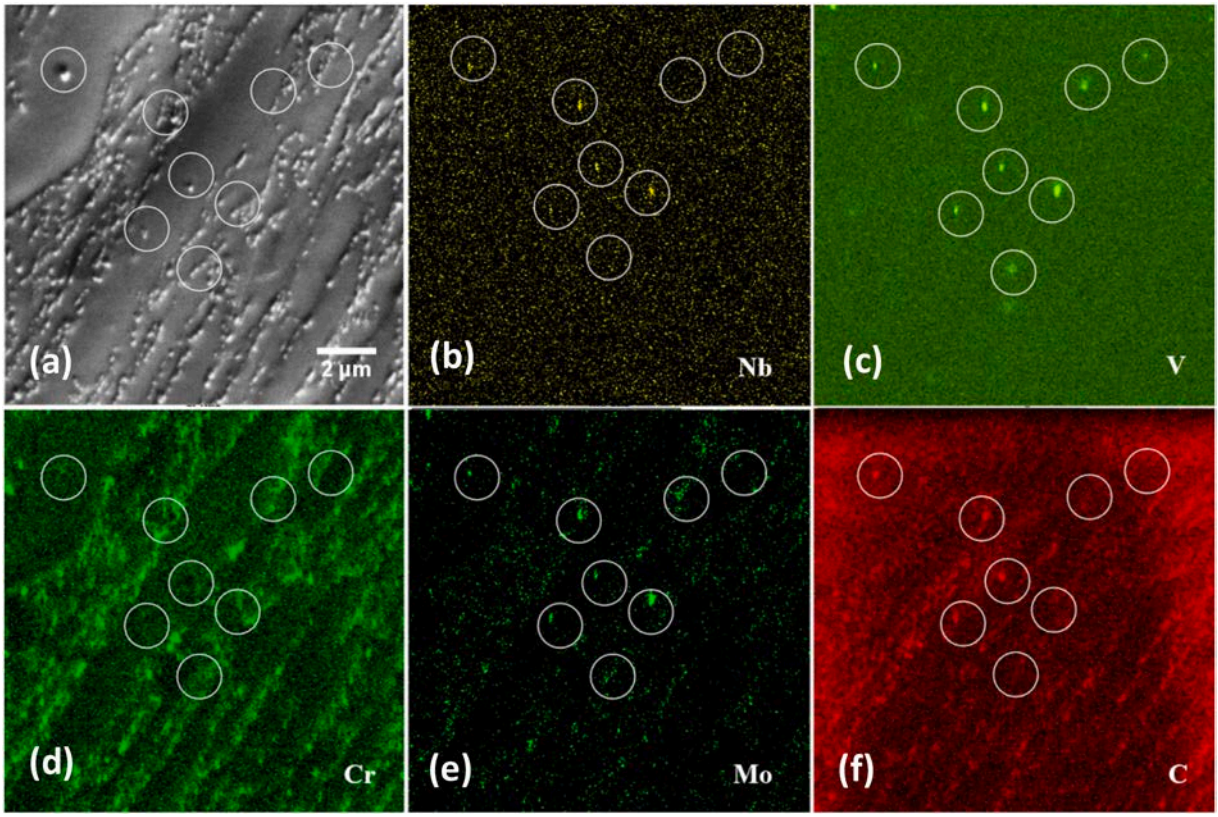

Fig. 9. SEM image including map scanning of the specimens after tempered at 700 °C for 2 h. (a) SEM image, (b-f) The distribution of Nb, V, Cr, Mo and C, respectively.

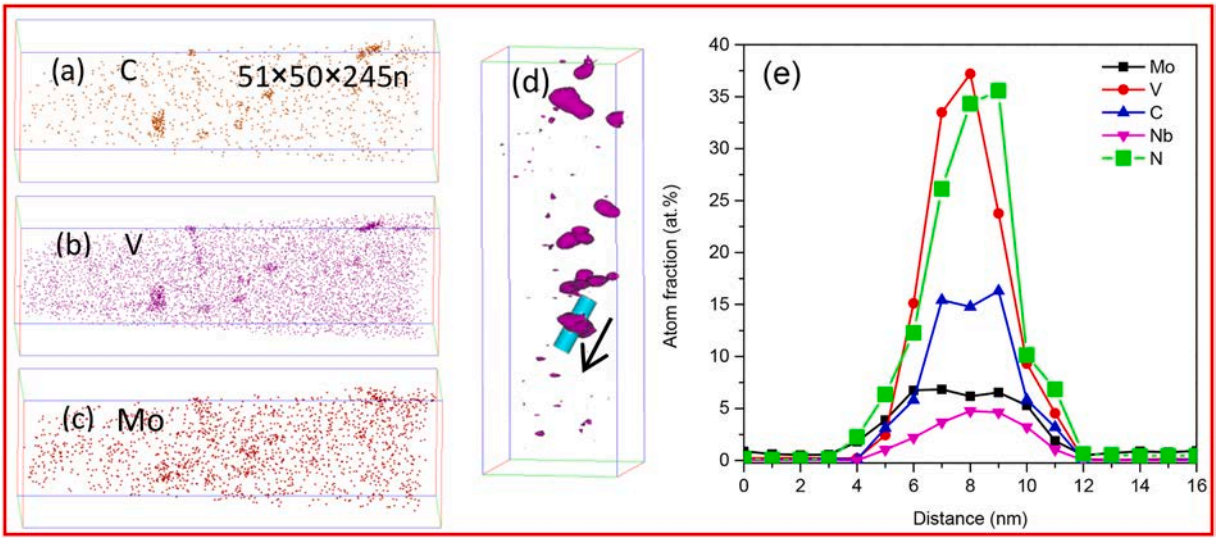

Fig. 10. (a-c) Atom maps showing the distribution of C, V, Mo in T700 condition, (d) The reconstructed ICS of 1.2 at.% V elements and the intercepted cylinder, and (e) the variation of element concentrations along the axis of the cylinder in Fig. 10d.

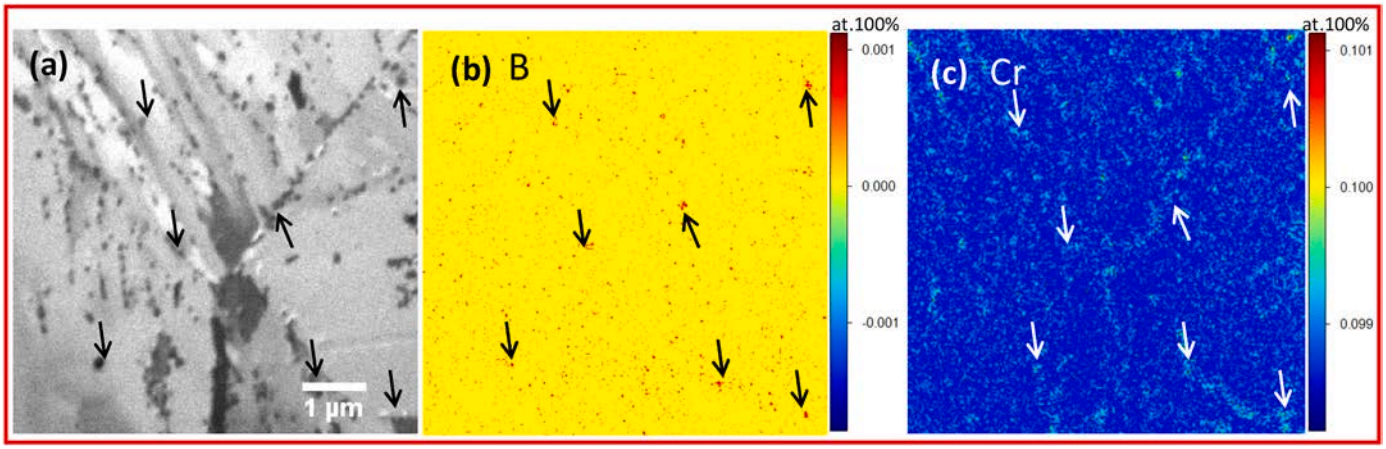

Fig. 11. SIMS analysis of FB2 steel in T700 condition: (a) FIB-SEM image, (b-c) the distribution of B and Cr elements, respectively.

ray studies by Jack indicate that the position of the C atom in the M_3C can be replaced by the B atom [22–24]. Physical explanation is that the entry of the B atoms into the existing gap position of interstitial compounds may reduce the number of three-dimensional electron [24]. On the other hand, the formation of M_3C carbides is accompanied by vacancies to adapt to changes in its local volume expansion [23]. And B atoms easily segregate into M_3C due to its strong combination with vacancies [24]. Therefore, the segregation of B and C occurs during tempering at 500 °C, forming $Fe_3(C,B)$ carbides.

After tempering at 600 °C, it was found that $(Cr,Mo)_2C$ and Cr-rich M_7C_3 particles distributed within martensitic lath, while Cr-rich $M_{23}C_6$ distributed at the martensite lath interfaces (Fig. 3a-d). The results of the APT analysis show that a large number of B atoms were enriched in the C + Cr + Mo + Mn and C + Mo + Cr clusters after tempering at 600 °C (Fig. 6–7). From the atomic ratio of these two clusters, it can be sure that the C + Cr + Mo + Mn and C + Mo + Cr clsuters are the M_7C_3 and M_2C carbides. Therefore, the precipitates in the T600 condition can be further identified as $(Cr,Mo)_2(C,B)$ and Cr-rich $M_7(C,B)_3$. As the tempering temperature increased to 700 °C, the $(Cr,Mo)_2(C,B)$ and Cr-rich M_7C_3 within martensitic lath were entirely replaced by Cr-rich $M_{23}C_6$ at the martensitic lath interfaces (Fig. 4b). And these $M_{23}C_6$ particles are rich in B atoms(Fig. 11) [25]. Therefore, the main precipitates formed during the tempering at 500 °C–700 °C are $Fe_3(C,B)$, $(Cr,Mo)_2(C,B)$, Cr-rich $M_7(C,B)_3$ and Cr-rich $M_{23}(C,B)_6$.

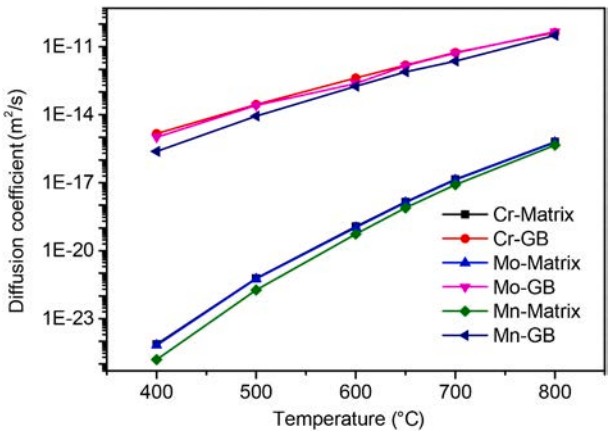

Fig. 12. The diffusion coefficients of Cr, Mo and Mn in the matrix and at grain boundaries of ferrite at different tempering temperatures in FB2 steel.

Normally, the formation and distribution of precipitates depend on elemental diffusion and its thermal stability, while the morphology

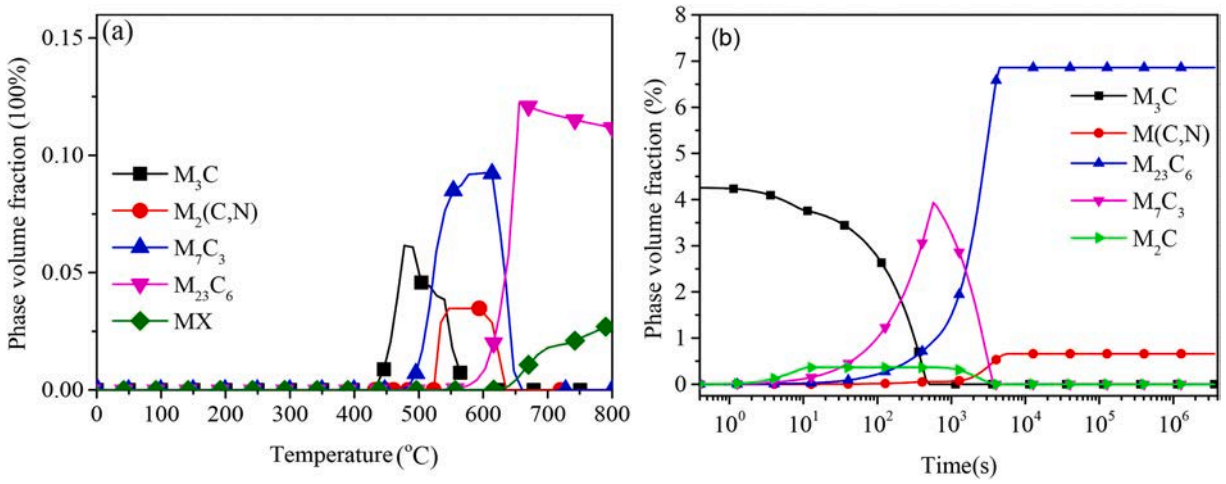

Fig. 13. The calculated results by Matcalc software: (a) The variation of precipitates phases fraction as a function of tempering temperatures with a heating rate 5 °C/min from 30 °C to 800 °C, (b) The volume fraction variation of phases as a function of holding time during tempering at 700 °C.

depends on their surface energy and strain energy [26]. It can be seen from Fig. 12 that the diffusion coefficients of Cr, Mn and Mo in ferrite increase considerably with the tempering temperature from 500 °C. And these diffusion coefficients at the grain boundaries is much higher than that in the interior of the matrix, due to the large lattice distortion caused by the irregular arrangement of atoms at the martensite lath interface. From this perspective, substitutional atoms are more easily segregated at the boundaries, resulting in precipitates at boundaries rich in Cr, Mn and Mo. In addition, M_2C and M_7C_3 have a smaller mismatch with the matrix than $M_{23}C_6$, indicating that $M_{23}C_6$ has larger strain energy [27]. Therefore, most M_2C and M_7C_3 with low substitution atomic ratio easily form within the martensitic lath in a long rod and shuttle shapes, respectively, caused by element diffusion and low strain energy. On the contrary, Cr-rich $M_{23}(C, B)_6$ with a high substitution atomic ratio and a large surface energy prefer to precipitate at boundaries in a spherical shape.

With the tempering temperature rising to 700 °C, the Gibbs free energy of M_2C and M_7C_3 increases gradually, leading to the decrease of

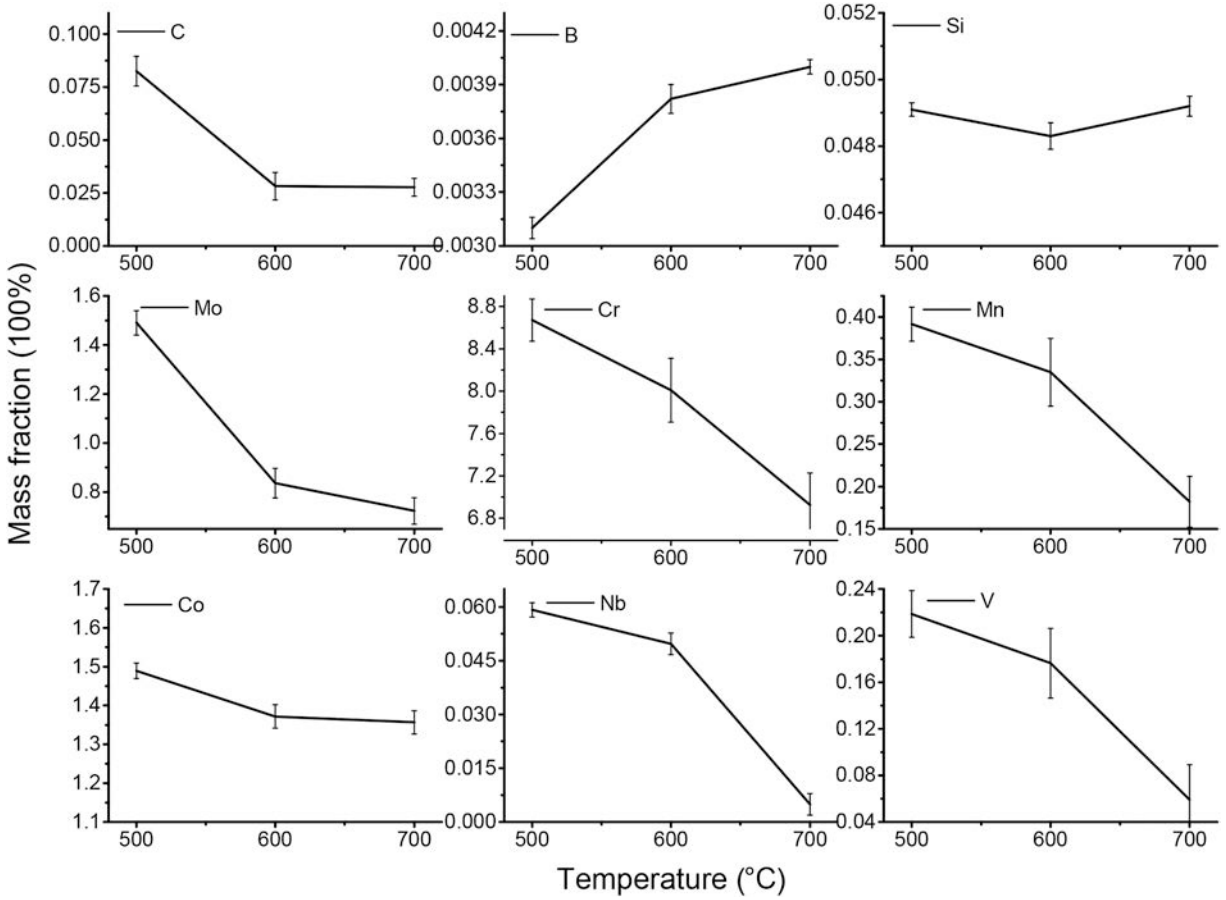

Fig. 14. The variation of elements concentration in the matrix obtained by APT as a function of tempering temperatures.

their thermal stability [28]. Further calculated result(Fig. 13a) indicates that martensite is first decomposed into M_3C, and then replaced by M_7C_3 and M_2C during tempering. With the increase of tempering temperature, these carbides in the matrix eventually evolved into relatively stable $M_{23}C_6$, which also also obtained through experiments and computer simulation by Djebaili [30] and Anders [31]. Besides, it can be seen from the calculation result(Fig. 13b) of tempering at 700 °C by Matcalc Software that the fraction of M_7C_3 reaches the maximum when the holding time reaches 600 s, and then reduces gradually. Subsequently, the fraction of $M_{23}C_6$ increases with the deduction of M_2C and M_7C_3 continuously, indicating that the diminishing of M_2C and M_7C_3 provide C and other elements for the formation of $M_{23}C_6$ at the martensitic lath interfaces. It is worth noting that there is only $M_{23}C_6$ and V(C, N) when the holding time is above 3000 s. Thus, the M_2C and M_7C_3 were not found in the T700 condition. Through in situ observation, it was found that the transformation of Cr-rich M_7C_3 to Cr-rich $M_{23}C_6$ was also observed in Cr–Mo–C steels during tempering at 700 °C [29]. As discussed above, the precipitation sequence in FB2 steel during tempering can be represented as follows: $Fe_3(C, B) \rightarrow (Cr, Mo)_2(C, B)$ + Cr-rich $M_7(C, B)_3 \rightarrow$ Cr-rich $M_{23}(C, B)_6$.

MX particles are observed in the T600 and T700 conditions(Fig. 3c, 4a, 8, 9, 10). However, the absence of MX in Q1100 and T500 conditions indicates that there are no undissolved particles during austenitization, and the MX cannot be formed during tempering 500 °C. From the results of EDS and APT(Fig. 4a, 8, 9, 10), it can be seen that the MX particles are rich in Nb, Mo, N and C. And the average atomic concentration of MX particles in is 31.67 V4.72Nb14.42Mo36.56N 13.45C(at.%) in the T600 sample and 37.48V4.76Nb6.38Mo35.58N13.85C(at.%) in the T700 sample. Thus, the MX precipitates in FB2 steel can be expressed as (V, Nb,Mo)(N,C). Y.Z. Shen [32] suggest that the composition of the MX is not only related to the chemical composition of the steel, but also the heat treatment conditions. By APT, Xu [17] demonstrated that M (C, N) type carbonitrides precipitated during tempering or long-term service of steel containing C and N elements, where M is Cr, V, Nb. While the experimental results by Orr and Woollard [33] indicated that the chemical formula of the MX type precipitate phase in 9CrNbVN steel under normalizing and tempering (1050 °C + 750 °C) conditions of can be expressed as (V0.6Cr0.3Fe0.1)N or (V0 .5Nb0.25Cr0.15Fe0.1)N, where M atoms can be Nb, Cr, Fe and W. In FB2 steel, the MX is the carbon-nitrogen type containing Mo, which may be due to the strong mutual attraction between Mo and N. As the tempering degree increases, Cr and Mo in (V, Nb, Mo) (N, C) were gradually replaced by V and Nb. Besides, although the size of MX increases with the enhancement of tempering temperature, this coarsening trend is not significant. These results are similar to those obtained in previous studies [34], showing that VN precipitates are highly resistant to coarsening. The physical explanation given in Ref [34], pointed out that the slow diffusivity of Nb and V may affect the coarsening rate of the carbide.

4.2. Elemental redistribution during tempering

Due to the low diffusion coefficients of substitutional atoms, the substitutional alloying elements can't have sufficient time to redistribute between carbides and the matrix in T500 condition. And the atomic probe statistic results(Fig. 14) show that the concentration of C in the matrix remains unchanged after tempering above 600 °C, indicating that the segregation of C in FB2 martensitic steel finished after tempering at 600 °C, which also has been proposed based on the electrical resistivity measurements in containing up to 0.2 wt% carbon steels [35].

APT and SMIS results (Fig. 5–7 and Fig. 11) show that B atoms are enriched in C clusters, which is different from the non-equilibrium segregation of B during quenching. During the quenching, B readily diffuses to the grain boundaries and interacts with vacancies due to the difference in free enthalpy of solute atoms between the matrix and the interface [8], thereby significantly reducing the total free energy of the system. However, the concentration of B in the matrix of FB2 steel increased first, and then remais unchanged (Fig. 14) during tempering, indicating that the segregation of B has the same variation trend as C. Karlsson [36] and M. Kurban [37] also found that B in 316L stainless steel diffused from grain boundaries into grains during tempering. Fang [38] suggests that this is due to the annihilation of the grain boundary vacancies during the tempering, resulting in the diffusion of free B atoms into the crystal. In this paper, the enrichment of B in C-clusters indicates that the formation and coarsening of carbides can provide spatial locations for the segregation of B atoms. And this is due to the volume expansion occurs during the formation and coarsening of precipitates such as M_3C and $M_{23}C_6$, so a large number of vacancies needs to adapt to its local volume changes. B atoms are easily dragged by the vacancy into these precipitates due to its high vacancy binding energy(0.48 eV) [8]. (See Fig. 7.)

According to the results of APT(Fig. 5), no segregation of Cr, Mn and Mo during tempering at low temperature(500 °C) was found. While previous studies show that the enrichment of Cr, Mn, Mo in M_3C was observed in Co-free 9Cr steels after tempering at 300–500 °C [18,39], which indicates that Cr, Mn, Mo in these steels have a higher diffusion coefficient than that in FB2 steel. For FB2 steel, the addition of 1.01 wt% Co can suppress the appearance of delta ferrite, residual austenite and reduce the coarsening rate of carbides during tempering [14], of which the reduction of carbide coarsening rate is achieved by reducing the diffusion coefficient of alloy elements and increasing the Curie transition temperature of the material [14,15]. Meanwhile, the addition of a certain amount of Co in the matrix will directly reduce the thermal vibration of Co in the matrix and increase the Orowan stress, due to the large Bohr magnetic moment of Co(1.72). And these two factors further decrease the diffusion coefficient of Cr, Mn, Mo in the matrix. From APT results in Figs.5-7, the Co atoms are enriched at the interfaces between carbides and matrix. Since Co is not a carbide forming element, this enrichment behavior can be considered that Co is extruded to the interface between carbides and matrix by the repulsive effect of carbon atoms during the formation of carbide, thereby further hindering the diffusion of Cr, Mn, Mo into carbides. Therefore, only $Fe_3(C, B)$ particles form in FB2 steel during tempering at 500 °C, because Co element may not only reduces the diffusion coefficient of the substitute alloy atoms but the enrichment of Co on the surface of cementite further hindered Cr, Mn, Mo entering cementite.

After tempering at 600 °C, two types of clusters(Cr + Mn + Mo + C + B and Mo + Cr + C + B) were observed, which indicate that Cr, Mn and Mo have different segregation behavior. Atomic probe statistics results (Fig. 14) further illustrate that the concentrations of Cr and Mn in the matrix decrease slowly at 500–600 °C and rapidly at 600–700 °C, while the concentration of Mo in the matrix remains unchanged after tempered above 600 °C. These results further confirm that these three elements have different segregation behavior, and the segregation of Mo is preferred over Cr and Mn during tempering. It is reported that the difference of alloying elements redistribution during tempering is determined by the diffusion coefficient of elements [40]. Further calculation results of the diffusion coefficients by Matcalc software (Fig. 12) indicates that the diffusion coefficient of Cr, Mn and Mo in matrix and grain boundaries(GB) of ferrite increases substantially with tempering temperature increase from 500 °C to 700 °C , but there is almost no difference among Cr, Mn and Mo in matrix or grain boundaries(GB) at the same temperature. It seems that the difference of diffusion coefficient in ferrite cannot be explained this difference of elemental segregation behavior. In fact, the diffusion coefficient of atoms is not only related to the lattice type, but also the interaction with other alloying elements. However, this factor has been ignored in the diffusion coefficient calculation.

J. D. pointed out that atoms' segregation also depends on its binding energy to vacancies (BEV) and the interaction coefficient between elements [41]. From the BEV and the interaction coefficient with carbon (IC) in Table 1, it can be known that BEV of C is about 0.54 eV, followed

Table 1
The vacancy binding energy(VBE) and interaction coefficient(α) with C of different elements calculated by Matcalc software.

Element	C	B	Cr	Mo	Mn
BEV(eV)	0.54	0.48	0.26	0.31	0.22
α(kJ/Mol)	-	-	−5	−16	−8

by B (0.48 eV), and both are much higher than Cr, Mo, Mn. This indicates that C is more easily interact with vacancy than B, and both have stronger interactions than Cr, Mo, and Mn. Besides, the interaction between elements is not negligible. Guttman believes that as the strength of mutual attraction of solutes increases, the tendency of co-segregation should become stronger [42]. It is well known that the interaction between substitutional atoms(M) and C atom can be expressed by the interaction coefficient α [42,43]. Since an attractive M-C interaction implies a negative coefficient, it gives rise to mutual enhancement of the adsorptions of C and M. Conversely, a repulsive interaction ($\alpha > 0$) reduces the adsorptions of both elements. From the given α data in Table. 1, it can be known that Mo has the stronger attraction with C than Cr and Mn. During tempering, these atoms interact with C, leading to the formation of carbides. Due to the higher binding energy of Mo and C, Mo segregated ahead of Cr and combine with C to form M_2C type carbide.

Non-carbide forming elements, such as Si and Co, can only change the dynamics, the morphology and distribution of precipitates [11–15]. The APT result of the T500 sample shows a clear indication of the partitioning of Si from cementite to ferrite, as Si has very low solubility in M_3C [11,12]. And thus, a high concentration flux of Si rejected from the cementite forms, which further affect the coarsening of M_3C. By tempering the sample at 600–700 °C, high concentrations of Si and Co are also found adjacent to carbon clusters/matrix interfaces, indicating that the solubility of these two elements in the M_2C, M_7C_3 and $M_{23}C_6$ is very small. Consequently, the flux of Co and Si in the opposite direction to that of C further rerard the coarsening of these carbides by hindering the substitutional atoms(Cr, Mo, Mn) into carbides. In addition, the concentration variation of Si and Co in the matrix remains unchanged with the increasing of tempering temperatures from 500 °C to 700 °C. Thus, the segregation of Si and Co during tempering is caused by the repulsive interaction of C to the carbides/matrix interfaces during tempering.

5. Conclusion

(1) Water-cooling after normalization at 1100 °C produces lathy martensite. During tempering at 500 °C, only the segregation of C and B occurs, forming needle-like $Fe_3(C,B)$. With enhancing the tempering temperatures from 600 °C to 700 °C, $(Cr,Mo)_2(C,B)$ and Cr-rich $M_7(C,B)_3$ within martensite lath were entirely replaced by Cr-rich $M_{23}(C,B)_6$ distributed at lath interfaces. Therefore, the precipitates sequence during tempering can be summarised as follows: $Fe_3(C,B)$ → $(Cr,Mo)_2(C,B)$ + Cr-rich $M_7(C,B)_3$ → Cr-rich $M_{23}(C,B)_6$.

(2) The segregation of Mo takes precedence over Cr and Mn, and Mo easily interact with C to form $(Cr,Mo)_2(C,B)$. In addition, Mo is also enriched in V clusters, forming (V, Nb, Cr, Mo) (N, C) particles as tempering temperature above 600 °C, and gradually replaced by Nb and V with the increase of tempering temperature from 600 °C to 700 °C.

(3) With the enhancing tempering temperature from 500 °C to 600 °C, the concentration of C in the matrix decreases gradually from 0.0825 at.% to 0.0282 at.%, while B increases from 30.3 ppm to 40.3 ppm. And then, both remain unchanged as tempering above 600 °C. But the concentration of Si and Co in the matrix remains unchanged during tempering, and both elements are rejected to the interfaces of carbides/matrix, forming a flux of Si and Co, which may retard the coarsening of carbides.

Declaration of Competing Interest

None.

Acknowledgement

This work was financilally supported by the National Key Research and Development Program of China (Grant No. 2018YF0702905).

References

[1] F. Abe, New martensitic steels, Mater. Ultra-Supercrit. Adv. Ultra-Supercrit. Power Plants (Jan. 2016) 323–374.
[2] B. Raj, M. Vijayalakshmi, Ferritic Steels and Advanced Ferritic-Martensitic Steels vol. 4, Elsevier Inc, 2012.
[3] K. Kaneko, K. Fujita, A. Sadakata, Y. Tomokiyo, S. Matsumura, Nanostructural and nanoelemental analysis of metastable M3C-type carbides with alloy-rich layer in heat resistant 2Cr-martensitic steel, Scr. Mater. 48 (6) (Mar. 2003) 761–765.
[4] N. Dudova, R. Kaibyshev, On the precipitation sequence in a 10%Cr steel under tempering, ISIJ Int. 51 (2011) 826–831.
[5] C. Pandey, A. Giri, M.M. Mahapatra, Evolution of phases in P91 steel in various heat treatment conditions and their effect on microstructure stability and mechanical properties, Mater. Sci. Eng. A 664 (2016) 58–74.
[6] J.M. Race, H.K.D.H. Bhadeshia, Precipitation sequences during carburisation of Cr–Mo steel, Mater. Sci. Technol. 8 (875–882) (1992) (United Kingdom).
[7] J. Janovec, M. Svoboda, A. Výrostková, A. Kroupa, Time-temperature-precipitation diagrams of carbide evolution in low alloy steels, Mater. Sci. Eng. A 402 (1–2) (2005) 288–293.
[8] J. Takahashi, K. Ishikawa, K. Kawakami, M. Fujioka, N. Kubota, Atomic-scale study on segregation behavior at austenite grain boundaries in boron- and molybdenum-added steels, Acta Mater. 133 (2017) 41–54.
[9] E.H. Jeong, S.G. Park, S.H. Kim, Y. Kim, Do. Evaluation of the effect of B and N on the microstructure of 9Cr-2W steel during an aging treatment for SFR fuel cladding tubes, J. Nucl. Mater. 467 (2015) 527–533.
[10] Y. Zheng, F. Wang, C. Li, Y. He, Dissolution and precipitation behaviors of boron bearing phase and their effects on hardenability and toughness of 25CrMoNbB steel, Mater. Sci. Eng. A 701 (2017) 45–55.
[11] G. Miyamoto, J.C. Oh, K. Hono, T. Furuhara, T. Maki, Effect of partitioning of Mn and Si on the growth kinetics of cementite in tempered Fe-0.6 mass% C martensite, Acta Mater. 55 (2007) 5027–5038.
[12] J.X. Dong, F. Siciliano, J.J. Jonas, W.J. Liu, E. Essadiqi, Effect of silicon on the kinetics of Nb(C, N) precipitation during the hot working of Nb-bearing steels, ISIJ Int. 40 (2000) 613–618.
[13] D. Delagnes, P. Lamesle, M.H. Mathon, N. Mebarki, C. Levaillant, Influence of silicon content on the precipitation of secondary carbides and fatigue properties of a 5%Cr tempered martensitic steel, Mater. Sci. Eng. A 394 (2005) 435–444.
[14] L. Helis, Y. Toda, T. Hara, H. Miyazaki, F. Abe, Effect of cobalt on the microstructure of tempered martensitic 9Cr steel for ultra-supercritical power plants, Mater. Sci. Eng. A 510–511 (2009) 88–94.
[15] Å. Gustafson, J. Ågren, Possible effect of co on coarsening of M23C6 carbide and Orowan stress in a 9% Cr steel, ISIJ Int. 41 (2001) 356–360.
[16] P. Michaud, D. Delagnes, P. Lamesle, M.H. Mathon, C. Levaillant, The effect of the addition of alloying elements on carbide precipitation and mechanical properties in 5% chromium martensitic steels, Acta Mater. 55 (2007) 4877–4889.
[17] Y. Xu, et al., Nano-sized MX carbonitrides contribute to the stability of mechanical properties of martensite ferritic steel in the later stages of long-term aging, Acta Mater. 175 (2019) 148–159.
[18] X. Tao, J. Gu, L. Han, Characterization of precipitates in X12CrMoWVNbN10-1-1 steel during heat treatment, J. Nucl. Mater. 452 (2014) 557–564.
[19] S. Ma, et al., Microstructure and crystallography of M_7C_3 carbide in chromium cast iron, Mater. Chem. Phys. 161 (2015) 65–73.
[20] W.B. Jones, C.R. Hills, D.H. Polonis, Microstructural evolution of modified 9Cr-1Mo steel, Metall. Trans. A. 22 (5) (1991) 1049–1058.
[21] L. Morsdorf, C.C. Tasan, D. Ponge, D. Raabe, 3D structural and atomic-scale analysis of lath martensite: effect of the transformation sequence, Acta Mater. 95 (2015) 366–377.
[22] M.E. Nicholson, Solubility of boron in Fe3C and variation of saturation magnetization, curie temperature, and lattice parameter of Fe3(C,B) with composition, Jom 9 (1) (1957) 1–6.
[23] K.H. Jack, Binary and ternary interstitial alloys III. the iron-carbon system: the characterization of a new iron carbide, in: Proceedings of the Royal Society of London. Series A, Mathematical and Physical Sciences 195, 1948, pp. 56–61, 1040.
[24] I.R. Shein, N.I. Medvedeva, A.L. Ivanovskii, Electronic and structural properties of cementite-type M3X (M=Fe, Co, Ni; X=C or B) by first principles calculations, Physica. Section B371 (1) (2006) 126–132.
[25] K.A. Taylor, Grain-boundary segregation and precipitation of boron in 0.2 percent carbon steels, Metall. Trans. A 23 (1992) 107–119.
[26] G.R. Booker, J. Norbury, Studies on the Occurrence, Morphology and Identity of Nitride Precipitates in Iron and Steel, Springer, Berlin Heidelberg, 1960.
[27] T. Matsunaga, et al., Creep lifetime and microstructure evolution in boron-added 9Cr–1Mo heat-resistant steel, Mater. Sci. Eng. A 760 (2019) 267–276.

[28] O. Prat, J. Garcia, D. Rojas, C. Carrasco, A.R. Kaysser-Pyzalla, Investigations on coarsening of MX and M23C6 precipitates in 12% Cr creep resistant steels assisted by computational thermodynamics, Mater. Sci. Eng. A 527 (2010) 5976–5983.
[29] A. Inoue, T. Masumoto, Carbide reactions (M3C→M7C3→M23C6→M6C) during tempering of rapidly solidified high carbon Cr-W and Cr-Mo steels, Metallurgical Transactions A 11 (5) (1980) 739–747.
[30] H. Djebaili, H. Zedira, A. Djelloul, A. Boumaza, Characterization of precipitates in a 7.9Cr-1.65Mo-1.25Si-1.2V steel during tempering, Mater. Charact. 60 (9) (Sep. 2009) 946–952.
[31] BjärboMats Anders, Hättestrand, Complex carbide growth, dissolution, and coarsening in a modified 12 pct chromium steel—an experimental and theoretical study, Metall. Mater. Trans. A (2001).
[32] Y.Z. Shen, S.H. Kim, C.H. Han, H.D. Cho, W.S. Ryu, TEM investigations of MN nitride phases in a 9% chromium ferritic/martensitic steel with normalization conditions for nuclear reactors, J. Nucl. Mater. 384 (1) (Jan. 2009) 48–55.
[33] J. Orr, L. Woollard, in: A. Strang, D.J. Gooch (Eds.), Microstructural Development and Stability in High Chromium Ferritic Power Plant Steels, The Institute of Materials, London, 1997, p. 53.
[34] Y.Z. Shen, et al., Vanadium nitride precipitate phase in a 9% chromium steel for nuclear power plant applications, J. Nucl. Mater. 374 (2008) 403–412.
[35] G. Krauss, Tempering of martensite in carbon steels, Phase Transform. Steels 2 (2012) 126–150.
[36] L. Karlsson, H. Nordén, Overview no. 63 non-equilibrium grain boundary segregation of boron in austenitic stainless steel—IV. Precipitation behaviour and distribution of elements at grain boundaries, Acta Metall. 36 (1) (1988) 35–48.
[37] M. Kurban, U. Erb, K.T. Aust, A grain boundary characterization study of boron segregation and carbide precipitation in alloy 304 austenitic stainless steel, Scr. Mater. 54 (6) (Mar. 2006) 1053–1058.
[38] F. Liu, D.H.R. Fors, A. Golpayegani, H.O. Andrén, G. Wahnström, Effect of boron on carbide coarsening at 873 K (600 °c) in 9 to 12 pct chromium steels, Metall. Mater. Trans. A Phys. Metall. Mater. Sci. 43 (11) (2012) 4053–4062.
[39] W.B. Jones, C.R. Hills, D.H. Polonis, Microstructural evolution of modified 9Cr-1Mo steel, Metall. Trans. A. 22 (5) (1991) 1049–1058.
[40] F. Abe, New martensitic steels. Materials for Ultra-Supercritical and Advanced Ultra-Supercritical Power Plants, Elsevier, 2017, https://doi.org/10.1016/B978-0-08-100552-1.00010-5.
[41] J.D. Whittenberger, M.A. Dayananda, Observation of the vacancy drag effect, J. Appl. Phys. 41 (2) (1970) 840.
[42] Ph. Dumoulin, M. Guttmann, The influence of chemical interactions between metallic and metalloid solutes on their segregation in α-Fe I: co-segregation at free surface studied by auger electron spectroscopy, Mater. Sci. Eng. 42 (80) (1980) 249–263.
[43] Dierk Raabe, et al., Interface Segregation in Advanced Steels Studied at the Atomic Scale. Microstructural Design of Advanced Engineering Materials, Wiley-VCH Verlag GmbH & Co. KGaA, 2013.